

Journal of Materials Chemistry A

Accepted Manuscript



This is an *Accepted Manuscript*, which has been through the Royal Society of Chemistry peer review process and has been accepted for publication.

Accepted Manuscripts are published online shortly after acceptance, before technical editing, formatting and proof reading. Using this free service, authors can make their results available to the community, in citable form, before we publish the edited article. We will replace this *Accepted Manuscript* with the edited and formatted *Advance Article* as soon as it is available.

You can find more information about *Accepted Manuscripts* in the [Information for Authors](#).

Please note that technical editing may introduce minor changes to the text and/or graphics, which may alter content. The journal's standard [Terms & Conditions](#) and the [Ethical guidelines](#) still apply. In no event shall the Royal Society of Chemistry be held responsible for any errors or omissions in this *Accepted Manuscript* or any consequences arising from the use of any information it contains.



Journal Name

ARTICLE

Oriented Two-dimensional Zeolitic Imidazolate Framework-L Membranes and their Gas Permeation Properties

Zhaoxiang Zhong,^{ab} Jianfeng Yao,^b Rizhi Chen,^{ab} Zexian Low,^b Ming He,^b Jefferson Zhe Liu^c and Huanting Wang^{*b}

Received 00th January 20xx,
Accepted 00th January 20xx

DOI: 10.1039/x0xx00000x

www.rsc.org/

A two-dimensional zeolitic imidazolate framework (ZIF), ZIF-L, with unique anisotropic pore system makes it an excellent material for investigating ZIF membranes with crystallographically preferred orientation and their effects on gas separation properties. A *b*-oriented ZIF-L membrane was successfully prepared from a randomly oriented seed layer. In contrast, a *c*-oriented ZIF-L crystal layer was attached to the support through the vacuum filtration in the presence of polyethyleneimine. After a short-time secondary growth, the oriented layer grew into a continuous membrane with a high degree of *c*-out-of-plane orientation. The gas separation studies demonstrated the orientation-dependent separation behavior. In the single gas permeation experiments, the *c*-oriented ZIF-L membrane has higher ideal selectivities of 8.1 for H₂/N₂ and 24.3 for H₂/CO₂ compared to the corresponding values of 3.9 and 5.5 for *b*-oriented ZIF-L membrane. The results of binary gas permeation showed decreased separation factors of *c*-oriented membrane, but were still much higher than those of *b*-oriented membrane. This work provides new insights into controlling ZIF membrane orientation for achieving desirable gas separation performance.

1. Introduction

As a result of the enormous flexibility in design and functionalization of the skeleton construction through choices of inorganic and organic components, metal-organic frameworks (MOFs) exhibit promises in a wide range of applications, e.g., gas storage,¹ gas adsorption and separation,²⁻⁴ catalysis and chemical sensors.⁵⁻⁶ The well-defined pores and ultrahigh porosity endow MOFs with ample opportunities for selective separation of various molecules. Therefore, the development of MOF membranes for gas separation has become one of the major foci in the field.⁷⁻¹⁰ Zeolitic imidazolate frameworks (ZIFs), a subclass of metal-organic frameworks, have zeolitic porous structures with hybrid frameworks consisting of inorganic metal ions coordinated with organic imidazolate ligands.¹¹⁻¹³ Typical ZIFs such as ZIF-7, ZIF-8, ZIF-22, ZIF-68, ZIF-69, ZIF-90 and ZIF-108 membranes have shown good gas selective adsorption properties due to their narrow pore size distribution and special diffusion pathways for guest molecules, and many ZIFs have been fabricated into membranes to examine their

separation properties.^{7-10, 14-16}

In the membrane preparation processes, like zeolite membranes, the secondary growth method has been widely used to grow MOF films on various porous substrates,^{7-9, 17} and it offers better control over membrane microstructure as compared to the in situ synthesis method¹⁸⁻²¹. The in situ direct synthesis is often difficult to fabricate the continuous and thin films due to a low density of nucleation sites of MOF crystals on porous supports.²²⁻²⁴ For the secondary growth technique, a seed layer is pre-attached to the support and subsequently grown to a continuous crystal layer under hydro- or solvothermal conditions. The most commonly used seeds are nanocrystals of desired MOF. They are deposited onto the substrate, typically by dip-coating, spin coating or manual assembly methods.²⁵⁻²⁶ For example, Venna et al. reported a ZIF-8 tubular membrane obtained by secondary growth of ZIF-8 film seeded by rubbing.²¹ The resulting membranes were 5-9 μm in thickness. To enhance the adhesion between seed crystals and support surface, a polymer binder is sometimes used. For instance, in the preparation of ZIF-7 membranes, ZIF-7 nanocrystals were synthesized and then redispersed in polyethyleneimine (PEI) solution.¹⁹ A dip-coating technique was used for the surface seeding, followed by the microwave-assisted secondary growth to prepare a compact ZIF-7 layer on the support.

Controlling crystal orientation has been one of the key strategies in tailoring membrane properties. The oriented membrane can be formed by controlling the orientation of the deposited seed layer. For instance, Lai et al. reported the formation of uniformly *b*-out-of-plane oriented MFI films by

^a State Key Laboratory of Materials-Oriented Chemical Engineering, National Engineering Research Center for Special Separation Membrane, Nanjing Tech University, Nanjing 210009, China.

^b Department of Chemical Engineering, Monash University, Clayton, Victoria 3800, Australia. Email: huanting.wang@monash.edu

^c Department of Mechanical and Aerospace Engineering, Monash University, Clayton, Victoria 3800, Australia

Electronic Supplementary Information (ESI) available: Vacuum filtration setup, binary gas separation equipment, SEM images, EDXS mapping, XRD patterns and water contact experiments. See DOI: 10.1039/x0xx00000x

secondary growth of *b*-oriented seed layers.²⁷⁻²⁸ It was achieved by using structure-directing agents that acted as crystal-shape modifiers to enable the necessary orientation of the seed layer and the appropriate balance between in-plane and out-of-plane growth rates during the secondary growth. Improved separation properties were achieved in ZSM-5 membranes, as demonstrated by high-flux, high-selectivity xylene isomer separation. This approach was extended to the synthesis of the ZIF films or membranes.^{18, 29-31} Li et al. fabricated *c*-out-of plane oriented ZIF-7 nanorods and microrods membrane through evolutionary selection in a van der Drift-type growth originating from randomly oriented seed layers.³⁰ PEI was used in the seeding solution to enhance the linkage between the seeds and the support. The oriented membrane exhibited an increase in selectivity with temperature, and the H₂ permeance of the oriented membrane was one tenth of the randomly oriented membrane due to the anisotropic pore structure of ZIF-7 crystals. Bux et al.¹⁸ prepared highly oriented ZIF-8 membrane by seeding and secondary growth. By dip-coating, randomly oriented ZIF-8 nanocrystals were attached to the surface of a porous α -alumina support in the assistance of PEI. After solvothermal treatment, a continuous and well-intergrown ZIF-8 layer was produced, which showed a sharp molecular sieve separation for an equimolar H₂/C₃H₈ mixture with a separation factor of above 300. A highly *c*-oriented and well intergrown ZIF-69 membrane was prepared by seeded secondary growth method.²⁹ Both the separation factor and permeance were better than the randomly oriented ZIF-69 prepared by the in-situ solvothermal method. Therefore, the fabrication of oriented ZIF thin films is particularly important for selective separation as ZIFs have multidimensional and anisotropic channel networks.

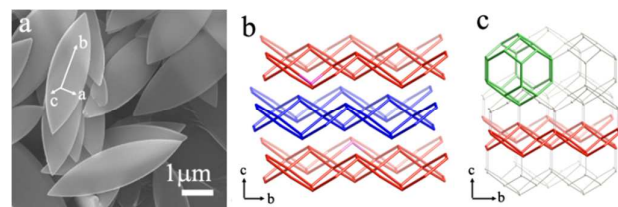


Fig. 1. a) SEM image of typical ZIF-L crystals, b) 2D layer structure of ZIF-L, and c) sod topology of ZIF-8.³²

Our group recently reported a new zeolitic imidazolate framework named as ZIF-L.³² The morphology of ZIF-L crystals is 2-dimensional leaf-shaped with the order of crystal dimensions $L_b > L_a \geq L_c$, where L_i denotes crystal length along the i axis (Fig. 1a). ZIF-L has a cushion-shaped cavity between layers with a dimension of 9.4 Å × 7.0 Å × 5.3 Å. The 2D layers stacking along the c direction are part of the sodalite (SOD) topology found in the 3D structure of ZIF-8 and there are six-membered ring and four-membered ring on them (Fig. 1b, c). The unique shape and pore systems of ZIF-L are very different from well-known MOF crystals.⁷⁻⁸ In this work, we aim to prepare ZIF-L membranes with two different orientations along its layered porous structure, i.e., *b*-oriented and *c*-oriented membranes,

and investigate their gas separation properties. To the best of our knowledge, this is the first example of direct growth of oriented, layered ZIF membranes. This work provides new insights into selective gas transport through layered ZIF structures, which will be useful for designing new ZIF materials for practical gas separation applications.

2. Experimental Section

2.1 Materials

Chemicals were used as received: Zn(NO₃)₂·6H₂O (98%), 2-methylimidazole (Hmim) (99%), branched polyethyleneimine (PEI; average Mw: ~25,000 by LS) and furfuryl alcohol (FA, ≥98%) were purchased from Sigma-Aldrich, Australia. Self-made porous α -Al₂O₃ disks with an average pore size of ca. 110 nm and a porosity of 35% were used as support for the ZIF-L membrane preparation. One side of the support was polished using a 1200 mesh SiC sandpaper. The other side of the support was wrapped with Teflon tape to avoid ZIF growth on it.

2.2 Preparation of *b*-oriented ZIF-L membrane

The *b*-oriented ZIF-L membrane was prepared by the dip-coating and secondary growth method. The seeding solution was prepared as follows: 0.59 g of Zn(NO₃)₂·6H₂O and 1.30 g of 2-methylimidazole (Hmin) were dissolved separately in 40 ml of water, and then two aqueous solutions were mixed together. The solution was stirred at 30 °C.³² After stirring for 0.5 h, the aforementioned support was dip-coated in the mixture and then dried at 80 °C for 2-3 h. Secondary growth was conducted using the same synthesis solution as that for the dip-coating. The ZIF-L seeded support was vertically placed in a beaker containing the synthesis solution and heated in an oven at 30 °C for 0.5-2 h. The resulting membrane was washed with deionized water and dried at 80 °C overnight. The secondary growth was repeated three times for some samples. To prove that the seeding is crucial for the ZIF-L membrane growth, a control experiment was conducted by using the bare alumina support to synthesize ZIF-L membrane at 30 °C for 2 h using the same synthesis solution.

2.3 Preparation of *c*-oriented ZIF-L membrane

Microsized 2D ZIF-L crystals were prepared and used to deposit on the alumina disk by a filtration deposition method, followed by secondary growth for a very short time to get a continuous membrane. ZIF-L crystals were synthesized as follows: 0.59 g of Zn(NO₃)₂·6H₂O and 1.30 g of Hmim were dissolved separately in 40 ml water, and then two aqueous solutions were mixed together. The solution was stirred at 30 °C for 1 h. The 2D ZIF-L crystals were collected by repeated centrifugation (at 8000 rpm for 5 min) and washed by deionized water for three times. A certain amount of above ZIF-L crystals was redispersed in 10 g of PEI aqueous solution (1.0 wt% PEI), and the suspension solution was vacuum-filtered with a porous Al₂O₃ support at a transmembrane pressure of 1 bar at room temperature (Fig. S1, Supplementary

Information). After the filtration, a highly *c*-oriented ZIF-L layer was deposited on the substrate. Secondary growth was done using the same synthesis solution as that for the ZIF-L crystals. The vacuum filtration seeded support was vertically placed in a beaker containing the synthesis solution and heated in an oven at 30 °C for 0.5 h. Then the solution was decanted off and the membrane was washed with deionized water, and then dried at 80 °C overnight.

2.4 Post-modification with PFA

A nonpermeable polymer material poly(furfuryl alcohol) (PFA) was chosen to fill grain boundaries.³³ PFA was prepared by dropwise adding 10 g of furfuryl alcohol (FA) into a solution containing 0.135 g of H₂SO₄ (98 wt%) and 10 g of ethanol, and then polymerization at 80 °C. To deposit PFA in the intercrystalline gaps, the obtained membranes were soaked in the PFA solution for 1 min and then dried at 60 °C for 2-3 h.

2.5 Membrane characterization

X-ray diffraction (XRD) of ZIF-L membranes was recorded on a Philips Vertical Diffractometer at 40 kV and 25 mA. Scanning electron microscopy (SEM) images were taken on a JEOL JSM 7001 microscope. Elemental mapping was performed using Energy-dispersive X-ray spectroscopy (EDX) on a JEOL JSM 7001 microscope.

2.6 Gas separation

The single gas permeation of membranes was measured using the pressure rise method. The feed side was maintained at 1 bar and the permeate side under vacuum. Permeate side pressure was monitored using a pressure transducer and was continuously recorded in a computer. The permeation setup was described in detail elsewhere.³⁴⁻³⁵ For the binary gas separation (Fig. S2), the flow rate of the feed gas was fixed at 100 ml min⁻¹ with 50 ml min⁻¹ for each gas (1:1 mixture). Argon was used as a sweep gas, and the sweep flow rate was set to 50 ml·min⁻¹. The measurements were conducted at room temperature. The gas composition was analyzed by a gas chromatograph (SRI 8610C gas chromatograph).

The permeance P_i of a single gas or a component in a mixture was calculated by:

$$P_i = \frac{N_i}{\Delta p_i A}$$

where N_i is the permeating flow rate of component i (mol/s), Δp_i the transmembrane pressure difference of component i (Pa), and A is the membrane area (m²). The gas selectivity S_{ij} is defined as the ratio of the two permeances P_i and P_j .³⁶

3. Results and discussion

3.1 Preparation of *b*-oriented ZIF-L film

After the dip-coating in the seed solution, the seeded support shows relatively weak XRD peaks before 2 θ of 20 ° (Fig. 2),

and the peak positions match well with those of simulated ZIF-L and ZIF-L powder. The weak XRD pattern of the seeded support indicates the ZIF-L seed layer is very thin. The comparison of the XRD patterns between the seed layer and the ZIF-L powder suggests the seed layer is composed of randomly stacked ZIF-L crystals.

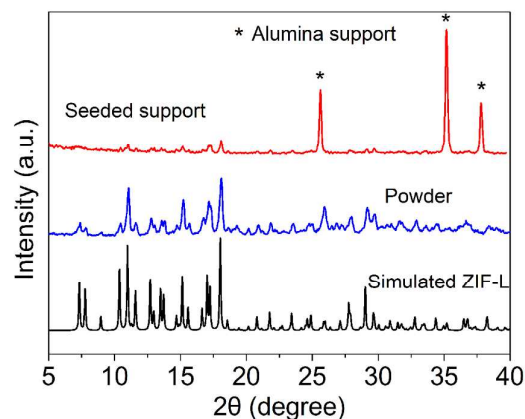


Fig. 2. XRD patterns of the simulated ZIF-L, ZIF-L powder and the seeded support.

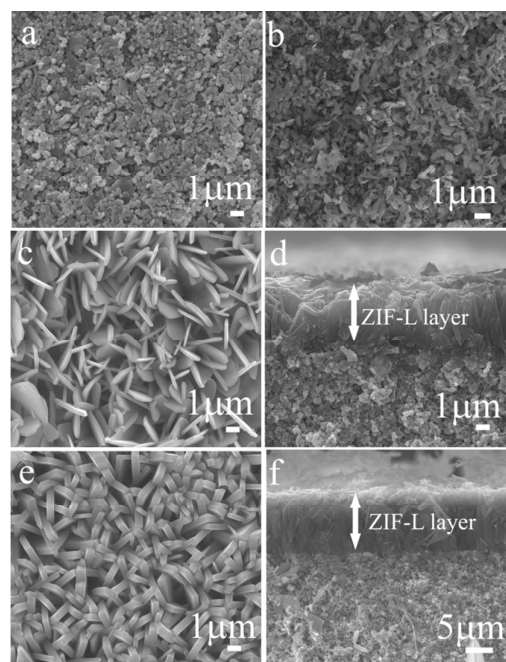


Fig. 3. SEM images of bare alumina support (a), seeded support (b) and ZIF-L membranes after secondary growth for 2 h (c,d), and with three times growth for 2 h each time (e, f). (a, b, c, e) surface and (d, f) cross-section.

SEM images of ZIF-L membranes supported on alumina disk at different stages are shown in Fig. 3. Compared with bare support surface (Fig. 3a), there are obvious crystals with a submicron size on the alumina support after dip-coating (Fig. 3b). However, the ZIF-L crystals on the support are not uniformly distributed, which may be due to the rough and uneven surface of the support. After 0.5 h of secondary growth, a continuous crystal layer is formed and the support is fully

covered (Fig. S3a). The leaf-shaped ZIF-L layer consisting of randomly oriented grains is observed after 1 h of secondary growth (Fig. S3b). Fig. 3c shows SEM image of the well-intergrown ZIF-L layer on alumina support after 2 h secondary growth. ZIF-L crystals have grown into integrated leaf-shaped crystals, which tend to form an oriented structure. The cross-section SEM image reveals a continuous and dense membrane with a thickness of about 5 μm (Fig. 3d). SEM image of the ZIF-L membrane grown on a bare alumina support using in situ growth method is shown in Fig. S3c. The membrane preparation without seeding results in a poorly intergrown film composed of randomly oriented grains. The low heterogeneous nucleation rate, resulting from the lower concentration of nuclei on the support, is not enough to grow a continuous film. This result demonstrates that seeding is necessary to prepare a continuous and dense ZIF-L layer on top of the alumina support.

After the growth of ZIF-L crystals, there were obviously some intercrystalline gaps on the membrane (Fig. 3c). The secondary growth was repeated for 3 times to fill the gaps. It can be seen from Fig. 3e that after multiple secondary growths, ZIF-L crystals intergrow more compactly and the sizes of the crystal gaps remarkably decrease. The cross-section SEM image of the membrane is shown in Fig. 3f. The ZIF-L layer is around 10 μm thick and all crystals grow with b axis perpendicular to the support surface; the ZIF-L layer becomes very dense and no crystal gaps are observed. Energy-dispersive X-ray spectroscopy (EDX) of the cross-section reveals a clear boundary between the ZIF-L layer (Zn signal) and the alumina support (Al signal) (Fig. S4).

XRD patterns of ZIF-L membranes prepared at various synthesis times are shown in Fig. 4. To estimate the degree of membrane orientation, the crystallographic preferred orientation (CPO) indexing method was used.^{18, 37-38} For the ZIF-L membrane prepared at 0.5-2 h, the XRD patterns are relatively weak but match well with the simulated ZIF-L, indicating a ZIF-L layer is successfully prepared. The CPO indexes, however, are still very low for the 1 h sample ($\text{CPO}_{020/112}=7.2$, $\text{CPO}_{020/004}=6.1$), indicating that a large amount of crystals are still randomly oriented.¹⁸ After repeated secondary growth (three times, 2 h each time), the (020) reflection increases remarkably and is already stronger than the (004) reflection, which dominates in the case of the randomly oriented powder (Fig. 2). The CPO indexes of the dominant (020) reflection in relation to the (112) ($\text{CPO}_{020/112}$) and the (004) reflections ($\text{CPO}_{020/004}$) are calculated to be 45.5 and 40.7, respectively, indicating the formation of strong b -out-of-plane orientation of ZIF-L crystals.³⁹

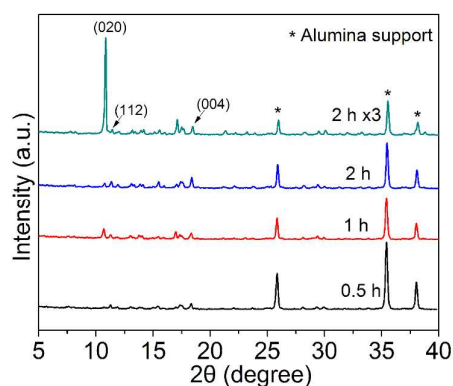


Fig. 4. XRD patterns of ZIF-L membrane prepared with secondary growth for 0.5, 1, 2 h, and repeated growth for three times with 2 h each.

The oriented growth of ZIF-L may be explained with the evolutionary selection (van der Drift growth) model⁴⁰⁻⁴¹, which is commonly used to explain oriented growth of zeolite membranes by the secondary growth method^{18, 30, 42}. The ratio of the average crystal length to the average crystal width is the most important factor in determining the CPO of the deposited layers according to evolutionary selection model. The morphology of these ZIF-L crystals is 2-dimensional leaf-shaped structure with the order of crystal dimensions $L_b > L_a \geq L_c$ (Fig. 1a), so the preferred orientation is attributed to the fastest growth along the b axis during the secondary growth. Schematic illustration of ZIF-L growth was shown in Fig. 5a. Starting from the randomly oriented ZIF-L seeds on a planar surface, the seeds grow into 2D leaf-shaped crystals with the same face-dependent growth rates. In the initial period, the continuous layer formed on the membrane surface is composed of randomly oriented crystals. By extending the secondary growth time, two possible processes are taken place. For the first type process, the ZIF-L crystals have the initial b axis perpendicular or nearly perpendicular to the support surface will keep their orientations along the b axis during the growth. For the second type process, the crystals with the b axis parallel or nearly parallel to the support surface will meet their lateral neighbors. As the growth rate along b axis is the fastest, in order to get enough growth space, they will “stand up” and turn their b axis upright to the substrate. The lateral growth along the c axis may also play an important role in the change of growth orientation.⁴⁰ Therefore, all the crystals should stand upright to the support if given enough growth time. Fig. 5b shows the enlarged cross-section SEM image of Fig. 3f, which indicates that the ZIF-L crystals in upper layer are perpendicular to the support surface (b axis), while those in lower layer deviate a little from b -orientation. This is strong evidence to support the evolutionary growth of ZIF-L crystals; the lower layer serves as the seeds for further secondary growth, contributing to the formation of a b -oriented top layer.⁴³

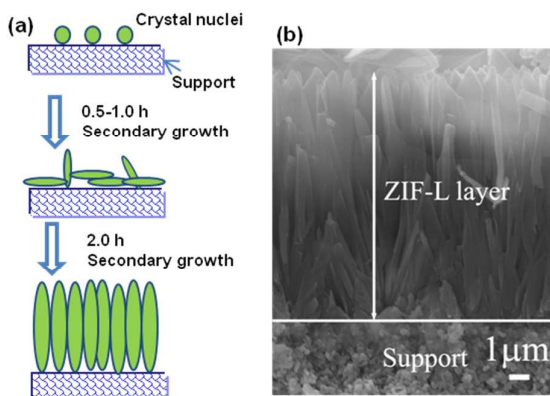


Fig. 5. Schematic illustration of *b*-oriented ZIF-L film formation (a) and the cross-section SEM image of ZIF-L film after three times growth (b, enlarged image of Fig. 3f).

3.2 Preparation of *c*-oriented ZIF-L film

Based on the above analysis, the randomly oriented seed layer always leads to the *b*-oriented ZIF-L membrane. So if ZIF-L crystals are deposited on the alumina support with *ab* plane parallel to the support (*c*-oriented), and the following secondary growth is strictly controlled to avoid the crystals standing up, the *c*-oriented membrane could be obtained. In our study, *c*-oriented ZIF-L layer was successfully obtained by depositing micro-sized ZIF-L nanoflakes with PEI as the binder on the substrate, and subsequent short secondary growth. As shown in the Fig. 6a, when the ZIF-L crystal suspension is vacuum filtrated, there is one normal force acting on the ZIF-L crystals in the immediate vicinity of the support, which is the drag force by the vacuum.⁴⁴ The drag force causes the solution transport to the support and deposit ZIF-L crystals on the surface with *ab* plane parallel to the support. The drag force also makes the ZIF-L layer pack densely to reduce the gaps between the crystals (Fig. 6b). As proposed by Ranjan and Tsapatsis,²⁶ PEI may form hydrogen bonds with both the ZIF crystals and free hydroxyl groups of the support surface. In addition, PEI may form Zn-N coordination bonds to zinc cations on the surface of the crystals. Therefore, addition of PEI to the seeding solution is vital to ensure that the seeding crystals strongly adhere to the support surface.

After secondary growth for 0.5 h at room temperature, the crystals in the *c*-oriented seed layer grow together and form a well-intergrown and continuous layer (Fig. 6c). However, after a long-time secondary growth (2 h), the crystals keep growing and then their orientation tends to change from *c*-orientation to *b*-orientation (Fig. S5), like the *b*-oriented ZIF-L growth illustrated in Fig. 5a. This is because most *ab* planes are not very strictly parallel to the substrate, and this deviation would be magnified with the extended secondary growth time. Another possible reason is that lateral growth often makes CPO deviate to the fastest growth direction.³⁰ Therefore, to obtain perfect *c*-oriented membrane, the secondary growth time should be strictly controlled.

The cross-sectional SEM image of the *c*-oriented membrane shows ZIF-L crystals deposited layer-by-layer with *ab* planes parallel to the support with a thickness of about 5 μm (Fig. 7a).

The thickness of the *c*-oriented ZIF-L layer could be simply controlled by changing the mass of crystals used in the vacuum depositing. The formation of the oriented ZIF-L layer on the support after 0.5 h secondary growth is confirmed by the XRD pattern as shown in Fig. 7b. Different to the randomly oriented XRD pattern of ZIF-L powder (Fig. 2), the oriented ZIF-L layer only shows (h00) peaks that correspond to [200], [400] and [800] planes of the ZIF-L, indicating a parallel orientation of the (h00) face to the substrate surface.

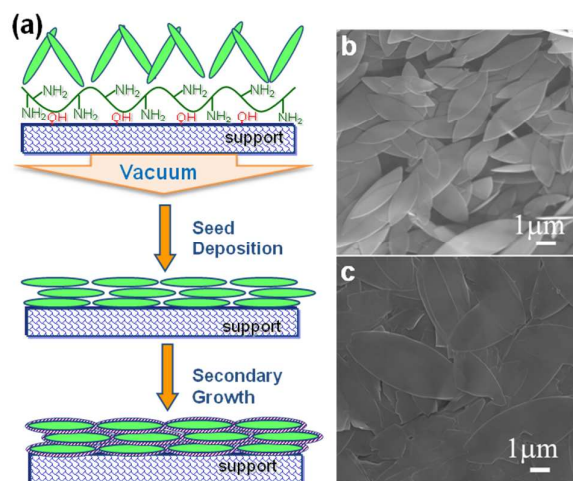


Fig. 6. Schematic illustration of PEI-assisted filtration-deposition of ZIF-L and the secondary growth (a), and SEM images of ZIF-L seeding after vacuum filtration (b) and ZIF-L membrane after 0.5 h secondary growth (c).

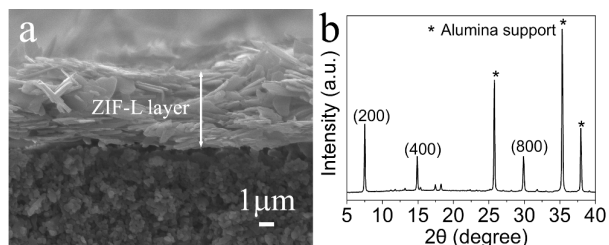


Fig. 7. (a) SEM cross-sectional image of *c*-oriented ZIF-L membrane, (b) XRD pattern of the *c*-oriented ZIF-L membrane.

3.3 Gas separation properties

The ZIF-L membranes were tested with single H₂, N₂ and CO₂ gases at 25 °C and the results are summarized in Table 1. For the *b*-oriented membrane (Fig. 3e), the ideal selectivity of H₂ over N₂ and CO₂ is 3.9 and 5.5 with a H₂ permeance of 4.2×10⁻⁷ mol·m⁻²·s⁻¹·Pa⁻¹, which exceeds the Knudsen selectivity of 3.7 and 4.7, respectively. The *c*-oriented membrane exhibits higher ideal selectivity for H₂ over N₂ (5.7) and CO₂ (10.4) as compared to *b*-oriented membrane. It is likely that the grain boundaries of the intercrystalline ZIF-L reduce the gas selectivity.⁴⁵ Polyfururyl alcohol (PFA) was chosen to fill inter-crystal pores since crosslinked PFA is gas impermeable.⁴⁶⁻⁴⁷ After PFA post-modification, both permeances of *b*-oriented and *c*-oriented membranes significantly decrease. But the ideal selectivity of *b*-oriented membrane does not change whereas

the ideal selectivity of *c*-oriented membranes increases significantly to 8.1 for H₂/N₂ and 24.3 for H₂/CO₂. This indicates that defect-free *b*-oriented membrane has been already formed before the post-modification, and the decreased permeances are attributed to deposition of dense PFA on the membrane surface; in the case of *c*-oriented membrane, the post-modification is shown to be effective for filling up ZIF-L intercrystal gaps. Compared to other ZIF membranes, the PFA-modified *c*-oriented ZIF-L membranes exhibited excellent gas separation properties (Table 1).

Table 1. Comparison of permeance and ideal selectivity of ZIF-L membranes and other ZIF membranes.

Sample	Permeance (10 ⁻⁸ mol·m ⁻² ·s ⁻¹ ·Pa ⁻¹)			Ideal selectivity		Ref.
	H ₂	N ₂	CO ₂	H ₂ /N ₂	H ₂ /CO ₂	
S _b -oriented	42.0	10.8	7.6	3.9	5.5	this work
S _c -oriented	84.6	14.9	8.1	5.7	10.4	this work
S' _b -oriented	16.9	4.4	3.2	3.8	5.3	this work
S' _c -oriented	19.5	2.4	0.8	8.1	24.3	this work
ZIF-7	7.4	1.1	1.1	6.7	6.7	19
ZIF-8	6	0.52	1.33	11.5	4.5	36
ZIF-8	36	9	13	4.0	2.8	48
ZIF-8	52	21	1.6	2.5	32.2	49
ZIF-8	113	25	-	4.6	-	50
ZIF-8	197	46	-	4.3	-	51
ZIF-90	30.8	-	4.1	-	7.5	3

S' represent the membranes after post-modification with PFA

To evaluate the gas separation properties of ZIF-L membranes after PFA post-modification in the purification and recycling of hydrogen from gas mixtures, gas separation experiments on equimolar binary gas mixtures (H₂/N₂ and H₂/CO₂) were carried out. The permeance and separation factors are summarized in Table 2. For the H₂/N₂ binary gas mixture separation, the H₂ permeance has a very small difference with that of the H₂ single gas permeance (Table 1), indicating the larger N₂ molecules only slightly influences the permeation of H₂. The H₂/N₂ separation factor is 3.8 for *b*-oriented ZIF-L membrane and 7.7 for *c*-oriented ZIF-L membrane. However, for the H₂/CO₂ binary gas mixture, the H₂/CO₂ separation factor is 4.9 for *b*-oriented ZIF-L membrane and 15.2 for *c*-oriented ZIF-L membrane, which is much lower than the H₂/CO₂ ideal selectivity. This phenomenon can be attributed to the competitive adsorption between H₂ and CO₂ in the membrane. The slowly diffused and strongly adsorbed CO₂ reduce H₂ transport through the membrane. On the contrary, the CO₂ diffusion through the membrane is also hindered to some extent by H₂ molecules. The *c*-oriented ZIF-L membrane shows better gas separation performance than the *b*-oriented ZIF-L membrane.

Table 2. Permeance and separation factor of ZIF-L membrane measured using equimolar binary gas mixtures.

Sample	Permeance(10 ⁻⁸ mol·m ⁻² ·s ⁻¹ ·Pa ⁻¹)				Separation factor	
	H ₂ -N ₂ pair		H ₂ -CO ₂ pair		H ₂ /N ₂	H ₂ /CO ₂
S' _b -oriented	15.5	4.1	6.3	1.3	3.8	4.9
S' _c -oriented	17.7	2.3	7.6	0.5	7.7	15.2

The gas separation data from single and binary gas mixture indicate the orientation of the ZIF-L crystals plays a major role in their selective separation. These results demonstrate the orientation-dependent separation behavior for ZIF-L membranes in the *b*-out-of-plane and *c*-out-of-plane orientations. The *c*-oriented ZIF-L thin layer with a smaller pore opening perpendicular to the support is favorable for the effective gas separation.

The orientation-dependent gas permeation through ZIF-L membrane is illustrated in Fig. 8. When *c* axis is perpendicular to the substrate, the 2D crystal layer ([h00] crystal plane) is parallel to the substrate surface. As indicated by the arrows in Fig. 8a, gas molecules driven by the transmembrane pressure, will pass from one layer to the adjacent layer. Fig. 8b, c show the six-membered ring windows and four-membered windows in the [200] plane. The size of these six-membered ring windows is the same as that of ZIF-8 and can be estimated to be 3.4 Å from rigid framework models, which is larger than the kinetic diameter of H₂ (2.89 Å), and CO₂ (3.3 Å), and smaller than N₂ (3.64 Å). And the contribution of the four-membered ring windows to mass transport through the pore network is presumably negligible because of the very small size.¹⁸ Therefore, the *c*-oriented ZIF-L membrane has the similar H₂ permeance to ZIF-8 membranes and high selectivities of H₂ over N₂ and CO₂.^{36, 52} Although N₂ has a kinetic diameter larger than the ZIF-L pore size (3.64 Å against 3.4 Å), it is able to permeate across the ZIF-L membrane. This indicates that the framework structure of ZIF-L is in fact more flexible. However, CO₂, despite having a kinetic diameter of only 3.3 Å and therefore being smaller than N₂, is found to permeate slower than N₂. This behavior is attributed to excellent CO₂ adsorption properties of the ZIF-L.³² The 2D layers of ZIF-L are weakly connected by the terminal Hmim-4 and "free" Hmim-5. These molecules are able to strongly coordinate with CO₂ gas,⁴⁹ resulting in an unusual reduction in CO₂ permeation rate.

When *b*-axis is perpendicular to support (Fig. 8d), the pathway that gas diffused through the ZIF-L is between the adjacent layers. From [020] crystal planes in the Figs. 8e and f, weakly connected crystal layers can be observed by the terminal Hmim-4 and "free" Hmim-5. As implied in our previous study,³² ZIF-L has cushion-shaped cavities between layers with a dimension of 9.4 Å × 7.0 Å × 5.3 Å. However, these cavities are dramatically different from those cages in the well-known ZIFs which have "fixed" pore openings. The terminal Hmim-4 and "free" Hmim-5 may have little hindrance effect on the gas diffusions. So the pathway that gas diffused could be the whole space between the layers, which is much larger than the kinetic diameters of H₂, N₂, and CO₂. Impressively, the ideal selectivity obtained from *b*-oriented

membrane are larger the corresponding Knudsen selectivity. This result could be ascribed to that the cavity in the ZIF-L is much more flexible than the tetrahedral structure of ZIFs. The real space that gas passed may shrink due to the compression with each other. In fact, molecular dynamics simulations revealed huge differences in diffusion coefficients of guest molecules in rigid and flexible ZIF structures.⁵³ A similar result was found to the HKUST-1 membranes. Even though HKUST-1 contains three dimensional channels of 9 Å in size surrounded by tetrahedral side pockets of 5 Å in size, the H₂/N₂ ideal selectivity of HKUST-1 membranes approached to the Knudsen selectivity.^{24, 45}

Because the pore systems of ZIF-L are three dimensions, the gas diffusion is not limited to one direction. As indicated in the Fig. 8a and d, a lateral diffusion also occurs. For *b*-oriented ZIF-L membrane, the molecule diffusion is not limited in the space between layers, but partially goes through the layers. So the six-membered ring windows in the layers also play a role. In this case, the lateral diffusion has a positive effect on the ideal selectivity. However, for *c*-oriented ZIF-L membrane, the lateral diffusion between layers also occurs, but this undesirable lateral diffusion is restricted for guest molecules because of the dense lateral stacking of layers,⁵⁴ and post-modification of the nonpermeable PFA.

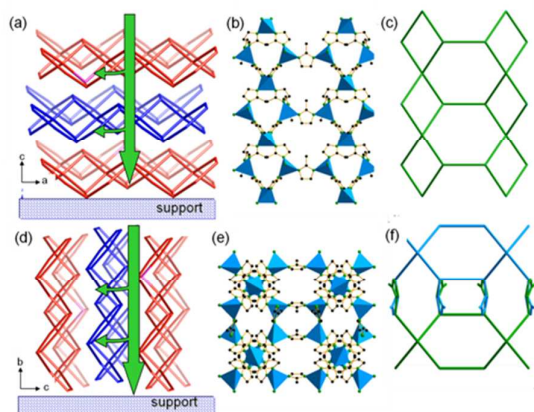


Fig. 8. Schematic illustration of the *c*-oriented ZIF-L membrane (a) and [200] crystal plane parallel to the support (b, c); Schematic illustration of the *b*-oriented ZIF-L membrane (d) and [020] crystal plane parallel to the support (e, f). The ZnN₄ tetrahedra are in blue and H atoms are omitted for clarity (b, e), the stick diagram (c, f).

Conclusions

The oriented ZIF-L membranes were prepared on the porous alumina support by secondary growth. The *b*-oriented membrane was obtained based on the dip-coating seeding method. Although the seed layer was randomly oriented, *b*-oriented ZIF-L film was obtained after the secondary growth. The highly oriented growth can be explained by the evolutionary selection model by van der Drift,⁴⁰⁻⁴¹ which predicts that the crystals' dimensions with the fastest growth survive. A filtration-deposition method was developed to prepare the *c*-oriented ZIF-L film. The *c*-oriented ZIF-L crystals

were attached on the alumina support through the vacuum filtration in the presence of PEI. After a short secondary growth, the oriented layer grew into a ZIF-L membrane with a preferential *c* orientation. Gas separation experiments showed that the oriented growth of ZIF-L had important effect on the permeation performance. The *c*-oriented membrane is more desirable than *b*-oriented membrane in terms of selectivity for H₂/N₂ and H₂/CO₂ due to the unique pore systems. Owing to its unique pore systems, ZIF-L membranes serve as a model system for theoretical study into mass transport through ZIFs, which would facilitate tailoring ZIF structure for practical applications.

Acknowledgements

This work is in part supported by the Australian Research Council (ARC). H.W. thanks ARC for a Future Fellowship. Z.Z. acknowledges the support from the National Natural Science Foundation of China (No. 21276124), and thanks the Monash University for hosting his visiting research.

Notes and References

- H. Wu, W. Zhou and T. Yildirim, *J. Am. Chem. Soc.*, 2007, **129**, 5314-5315.
- D. M. D'Alessandro, B. Smit and J. R. Long, *Angew. Chem. Int. Ed.*, 2010, **49**, 6058-6082.
- A. S. Huang, N. Y. Wang, C. L. Kong and J. Caro, *Angew. Chem. Int. Ed.*, 2012, **51**, 10551-10555.
- J. R. Li, Y. G. Ma, M. C. McCarthy, J. Sculley, J. M. Yu, H. K. Jeong, P. B. Balbuena and H. C. Zhou, *Coord. Chem. Rev.*, 2011, **255**, 1791-1823.
- H. L. Jiang, B. Liu, T. Akita, M. Haruta, H. Sakurai and Q. Xu, *J. Am. Chem. Soc.*, 2009, **131**, 11302-11303.
- G. Lu and J. T. Hupp, *J. Am. Chem. Soc.*, 2010, **132**, 7832-7833.
- D. Zacher, O. Shekhan, C. Woll and R. A. Fischer, *Chem. Soc. Rev.*, 2009, **38**, 1418-1429.
- A. Betard and R. A. Fischer, *Chem. Rev.*, 2012, **112**, 1055-1083.
- J. F. Yao and H. T. Wang, *Chem. Soc. Rev.*, 2014, **43**, 4470-4493.
- S. L. Qiu, M. Xue and G. S. Zhu, *Chem. Soc. Rev.*, 2014, **43**, 6116-6140.
- R. Banerjee, A. Phan, B. Wang, C. Knobler, H. Furukawa, M. O'Keeffe and O. M. Yaghi, *Science*, 2008, **319**, 939-943.
- H. Hayashi, A. P. Cote, H. Furukawa, M. O'Keeffe and O. M. Yaghi, *Nat. Mater.*, 2007, **6**, 501-506.
- B. Wang, A. P. Cote, H. Furukawa, M. O'Keeffe and O. M. Yaghi, *Nature*, 2008, **453**, 207-211.
- V. I. Isaeva, M. I. Barkova, L. M. Kustov, D. A. Syrtsova, E. A. Efimova and V. V. Teplyakov, *J. Mater. Chem. A*, 2015, **3**, 7469-7476.
- Y. J. Ban, Y. S. Li, Y. Peng, H. Jin, W. M. Jiao, X. L. Liu and W. S. Yang, *Chem. Eur. J.*, 2014, **20**, 11402-11409.
- A. Kasik, X. L. Dong and Y. S. Lin, *Microporous Mesoporous Mater.*, 2015, **204**, 99-105.
- C. M. Lew, R. Cai and Y. S. Yan, *Accounts Chem. Res.*, 2010, **43**, 210-219.
- H. Bux, A. Feldhoff, J. Cravillon, M. Wiebcke, Y. S. Li and J. Caro, *Chem. Mater.*, 2011, **23**, 2262-2269.

19. Y. S. Li, F. Y. Liang, H. Bux, A. Feldhoff, W. S. Yang and J. Caro, *Angew. Chem. Int. Ed.*, 2010, **49**, 548-551.
20. J. P. Nan, X. L. Dong, W. J. Wang and W. Q. Jin, *Microporous Mesoporous Mater.*, 2012, **155**, 90-98.
21. S. R. Venna and M. A. Carreon, *J. Am. Chem. Soc.*, 2010, **132**, 76-78.
22. M. Arnold, P. Kortunov, D. J. Jones, Y. Nedellec, J. Karger and J. Caro, *Euro. J. Inorg. Chem.*, 2007, 60-64.
23. J. Gascon, S. Aguado and F. Kapteijn, *Microporous Mesoporous Mater.*, 2008, **113**, 132-138.
24. J. P. Nan, X. L. Dong, W. J. Wang, W. Q. Jin and N. P. Xu, *Langmuir*, 2011, **27**, 4309-4312.
25. D. M. Jiang, A. D. Burrows, Y. L. Xiong and K. J. Edler, *J. Mater. Chem. A*, 2013, **1**, 5497-5500.
26. R. Ranjan and M. Tsapatsis, *Chem. Mater.*, 2009, **21**, 4920-4924.
27. Z. P. Lai, G. Bonilla, I. Diaz, J. G. Nery, K. Sujaoti, M. A. Amat, E. Kokkoli, O. Terasaki, R. W. Thompson, M. Tsapatsis and D. G. Vlachos, *Science*, 2003, **300**, 456-460.
28. Z. P. Lai, M. Tsapatsis and J. R. Nicolich, *Adv. Funct. Mater.*, 2004, **14**, 716-729.
29. Y. Y. Liu, G. F. Zeng, Y. C. Pan and Z. P. Lai, *J. Membr. Sci.*, 2011, **379**, 46-51.
30. Y. S. Li, H. Bux, A. Feldhoff, G. L. Li, W. S. Yang and J. Caro, *Adv. Mater.*, 2010, **22**, 3322-3326.
31. C. T. Hou, Q. Xu, J. Y. Peng, Z. P. Ji and X. Y. Hu, *Chemphyschem*, 2013, **14**, 140-144.
32. R. Z. Chen, J. F. Yao, Q. F. Gu, S. Smeets, C. Bärlocher, H. X. Gu, D. R. Zhu, W. Morris, O. Yaghi and H. T. Wang, *Chem. Commun.*, 2013, **95**, 9500-9502.
33. H. T. Wang, L. M. Huang, B. A. Holmberg and Y. S. Yan, *Chem. Commun.*, 2002, 1708-1709.
34. L. He, D. Li, D. H. Dong, J. F. Yao, Y. Huang and H. T. Wang, *Journal of Applied Polymer Science*, 2012, **124**, 3383-3391.
35. Y. S. Yan, M. E. Davis and G. R. Gavalas, *Ind. Eng. Chem. Res.*, 1995, **34**, 1652-1661.
36. H. Bux, F. Y. Liang, Y. S. Li, J. Cravillon, M. Wiebcke and J. Caro, *J. Am. Chem. Soc.*, 2009, **131**, 16000-16001.
37. A.-J. B. J.P. Verduijn, M.H.C. Anthonis, L.R. Czarnetzki, *WO 96/01683*, 1996.
38. H. K. Jeong, J. Krohn, K. Sujaoti and M. Tsapatsis, *J. Am. Chem. Soc.*, 2002, **124**, 12966-12968.
39. Y. Yoo, Z. P. Lai and H. K. Jeong, *Microporous Mesoporous Mater.*, 2009, **123**, 100-106.
40. A. J. Bons and P. D. Bons, *Microporous Mesoporous Mater.*, 2003, **62**, 9-16.
41. Vanderdr.A, *Philips Res. Rep.*, 1967, **22**, 267-288.
42. J. Caro, M. Noack and P. Kolsch, *Adsorption*, 2005, **11**, 215-227.
43. J. Choi, S. Ghosh, Z. P. Lai and M. Tsapatsis, *Angew. Chem. Int. Ed.*, 2006, **45**, 1154-1158.
44. Z. X. Zhong, W. H. Xing, X. Liu, W. Q. Jin and N. P. Xu, *J. Membr. Sci.*, 2007, **301**, 67-75.
45. V. V. Guerrero, Y. Yoo, M. C. McCarthy and H. K. Jeong, *J. Mater. Chem.*, 2010, **20**, 3938-3943.
46. M. B. Shiflett and H. C. Foley, *Science*, 1999, **285**, 1902-1905.
47. H. T. Wang, L. X. Zhang and G. R. Gavalas, *J. Membr. Sci.*, 2000, **177**, 25-31.
48. Y. C. Pan and Z. P. Lai, *Chem. Commun.*, 2011, **47**, 10275-10277.
49. G. S. Xu, J. F. Yao, K. Wang, L. He, P. A. Webley, C. S. Chen and H. T. Wang, *J. Membr. Sci.*, 2011, **385**, 187-193.
50. M. He, J. F. Yao, L. X. Li, Z. X. Zhong, F. Y. Chen and H. T. Wang, *Microporous Mesoporous Mater.*, 2013, **179**, 10-16.
51. J. F. Yao, D. H. Dong, D. Li, L. He, G. S. Xu and H. T. Wang, *Chem. Commun.*, 2011, **47**, 2559-2561.
52. M. C. McCarthy, V. Varela-Guerrero, G. V. Barnett and H. K. Jeong, *Langmuir*, 2010, **26**, 14636-14641.
53. L. Hertag, H. Bux, J. Caro, C. Chmelik, T. Remsungnen, M. Knauth and S. Fritzsche, *J. Membr. Sci.*, 2011, **377**, 36-41.
54. B. Liu, M. Tu and R. A. Fischer, *Angew. Chem. Int. Ed.*, 2013, **52**, 3402-3405.

TOC

b- and *c*-oriented ZIF-L membranes were synthesized by controlling ZIF-L orientational growth, and they showed orientation-dependent gas permeation properties.

